

Differential cross sections and polarization of $H\alpha$ in $H^+ + H$ collisions

C Balança[†], C D Lin[‡] and N Feautrier[†]

[†] DAMAp and URA 812 du CNRS, Observatoire de Paris, 92195 Meudon Cedex, France

[‡] Department of Physics, Kansas State University, Manhattan, KS 66506, USA

Received 3 November 1997

Abstract. The presence of an axially symmetric angular distribution of energetic protons in astrophysical plasmas can be detected by measuring the linear polarization of the lines emitted from collisionally excited levels of atoms. Another signature of proton beams can be found in the study of line profiles. For a quantitative interpretation of the observations of the $H\alpha$ line one needs to know all the relevant integrated and differential cross sections and the polarization fraction.

Coupled-state calculations based on a two-centre expansion in atomic orbitals and pseudostates were carried out for protons colliding with $H(1s)$ in the impact energy range 1–100 keV. Differential cross sections for excitation and capture from the level $n = 1$ to the level $n = 3$ as well as the total and differential polarization fraction of the $H\alpha$ line are presented. It is shown that the differential cross sections reach a maximum for an angle varying from 1 to 10^{-2} degree when the collision energy varies from 1 to 40 keV. For 1 keV collisions, this leads to large recoil velocities and, as a consequence, to a large Doppler broadening. At the same energy, the resulting polarization fraction is found to have only small variations with the deflection angle.

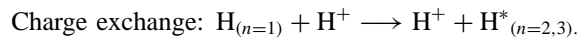
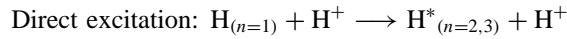
1. Introduction

Collisions between protons and hydrogen atoms have been extensively studied in the past 30 years, in both the experimental and theoretical fields. These collisions also frequently occur in astrophysical environments and theoretical results are needed to interpret phenomena such as those occurring in solar flares, for example, the broadening, shift of the line emitted by the excited atoms and the polarization of the radiation measured during these events. It has been shown (Hénoux *et al* 1990) that flares produce some particle beams that collide with chromospheric hydrogen atoms. Electrons are detected through the radio, x-ray and γ -ray emission and through the enhancement of the visible and UV emission continua produced by their interaction with the solar atmosphere. High-energy protons produce γ -ray emission by bombarding the solar atmosphere and are also detected in interplanetary space, but low-energy protons are more difficult to detect. The first technique is based on the measurement of the polarization of atomic lines resulting from bombardment in the lower atmosphere by protons with an anisotropic velocity distribution. Linear polarization of the hydrogen $H\alpha$ line was observed in some chromospheric flares and interpreted as being due to bombardment, by either low-energy protons (1–40 keV) or neutral beams carrying both protons and electrons (Hénoux *et al* 1990).

Another signature of proton bombardment can be found in the enhancement of the red wing of chromospheric lines, due to Doppler-shifted emission of the neutral hydrogen

atoms formed by charge exchange (Fang *et al* 1995). This effect is probably small in the case of the H α line, but is expected to be significant in the red wings of the Ly α and Ly β lines. Moreover, the recoil motion of the H atoms after excitation gives rise to a macroscopic Doppler broadening of the emitted lines. The line profiles are thus a function of the velocity distribution of the incoming beam and are directly related to the differential excitation cross sections.

In the near future, spectropolarimetric observations of the H α line will be obtained with the French–Italian Solar Telescope THEMIS. For detailed modelling of these observations at high spectral resolution, one will need to know all the relevant differential cross sections for excitation and capture that are presently unknown. The aim of this work is to investigate what predictions can be made for the differential cross sections and polarization fractions for direct excitation and charge exchange for the following processes in proton–atomic hydrogen collisions:



Section 2 briefly outlines the close-coupling approach and gives the basis set used to calculate all the cross sections. The integral cross sections and the polarization are presented in section 3 and compared with available experimental results. Section 4 concentrates on differential cross sections and polarization. We conclude in section 5.

2. Theory

An atomic orbital basis is adapted for the energy range investigated and so we use the two-centre atomic-orbital (TCAO) close-coupling method established by Bates and McCarroll (1958), Wilets and Gallaher (1966), Cheshire *et al* (1970) and Fritsch and Lin (1982). This allows us to obtain the amplitudes and the partial cross sections of the different sublevels of $n = 2$ and $n = 3$ needed for both differential cross sections and polarization fractions.

2.1. Charge exchange and close-coupling

Within the semiclassical impact-parameter approximation, the time-dependent wavefunction $\Psi(\vec{r}, t)$ is expanded in terms of bound atomic orbitals and continuum states including the plane-wave electronic translational factors. The time-dependent electronic wavefunction is given by

$$\begin{aligned} \Psi(\vec{r}, t) = & \sum_p a_p(t) \phi_p^A(\vec{r}_A) \exp\left(i\frac{\vec{v} \cdot \vec{r}}{2} - i\frac{v^2}{8}t - i\alpha_p t\right) \\ & + \sum_q b_q(t) \phi_q^B(\vec{r}_B) \exp\left(-i\frac{\vec{v} \cdot \vec{r}}{2} - i\frac{v^2}{8}t - i\beta_q t\right) \end{aligned} \quad (1)$$

where particle A is the incident proton, i.e. the projectile, and particle B is the proton of the initial hydrogen atom, i.e. the target. $a_p(t)$ and $b_q(t)$ are the transition amplitudes for the occupation of atomic states $\phi_p^A(\vec{r}_A)$ and $\phi_q^B(\vec{r}_B)$ that have the respective eigenenergies α_p and β_q . We have first performed a traditional symmetric TCAO close-coupling calculation (S). The basis set (TCAO-S) includes 26 states on each centre of this symmetric collision, allowing us to describe the sublevels 1s–4d₂. Furthermore it includes other bound states and pseudostates to take the continuum into account as shown in table 1.

Table 1. The 26 states of the basis set with their respective eigenenergies obtained by diagonalizing the Hamiltonian. The pseudostates have a positive eigenenergy.

ns	E (au)	$n\mathbf{p}_m$	E (au)	nd_m	E (au)
1s	-0.500 000	2p ₀	-0.125 000	3d ₀	-0.055 556
2s	-0.125 000	3p ₀	-0.055 556	4d ₀	-0.031 206
3s	-0.055 556	4p ₀	-0.031 240	3d ₁	-0.055 556
4s	-0.031 244	5p ₀	-0.000 418	4d ₁	-0.031 206
5s	-0.008 621	6p ₀	0.205 341	3d ₂	-0.055 556
6s	0.096 508	7p ₀	1.524 853	4d ₂	-0.031 206
7s	0.570 062	2p ₁	-0.125 000		
8s	3.962 578	3p ₁	-0.055 556		
		4p ₁	-0.031 240		
		5p ₁	-0.000 418		
		6p ₁	0.205 341		
		7p ₁	1.524 853		

However, as shown by Slim and Ermolaev (1994) and Kuang and Lin (1996a, b), the TCAO close-coupling cross sections exhibit spurious oscillatory structures that are absent in the experimental data (Park *et al* 1976, Detleffsen *et al* 1994). These structures, due to the representation of the continuum by short-range pseudostates, are removed by including pseudocontinuum states at only one centre. Thus, to obtain a better agreement for the excitation cross sections and the polarization fraction, we have performed an asymmetric TCAO close-coupling calculation (A), in which all the pseudostates on the projectile centre have been removed. The basis set (TCAO-A) includes 26 states on the target centre B and only 19 bound states on the projectile A.

2.2. Differential cross section and polarization

The partial and total cross sections are easily obtained from the transition amplitudes for capture:

$$\sigma_{if}^A(E) = 2\pi \int_0^\infty db b |a_f(b, Z_0)|^2 \quad (2)$$

and direct excitation:

$$\sigma_{if}^B(E) = 2\pi \int_0^\infty db b |b_f(b, Z_0)|^2. \quad (3)$$

The differential cross sections are given by

$$\frac{d\sigma_{if}(\theta, E)}{d\Omega} = |f_{if}^{A,B}(\theta, E)|^2 \quad (4)$$

where the scattering amplitude is

$$f_{if}^{A,B}(\theta, E) = m_p v (-i)^{\Delta m + 1} \int_0^\infty db b J_{\Delta m}(\eta b) (T_{if}^{A,B}(b, Z_0) - \delta_{if}) \quad (5)$$

m_p is the mass of the proton, v the relative velocity, $\Delta m = |m_f - m_i|$ is the difference between the initial and final magnetic quantum numbers, $J_{\Delta m}$ is the Bessel function of integer order Δm , while $\eta = 2m_p v \sin(\theta/2)$ and $Z_0 = vt$ is the limit of integration for the coupled equations ($Z_0 \rightarrow \infty$). $T_{if}^{A,B}(b)$ is the transition amplitude from a state i of B to a state j of A or B for an impact parameter b , with initial conditions $b_q(b, -\infty) = \delta_{qi}$ and

$a_p(b, -\infty) = 0$. The transition amplitude must include the Coulomb phase factor as shown by Dubois *et al* (1993). In the case of capture to a state j of A , the amplitude is given by

$$T_{if}^A(b, Z_0) = a_f(b, Z_0) \exp\left(\frac{i}{v} \left[2 \ln(b) - 2 \ln\left(\sqrt{Z_0^2 + b^2} + Z_0\right) \right]\right). \quad (6)$$

In the case of direct excitation the expression is the same as (6), with amplitude a_f changed into b_f . As the hydrogen atoms are initially in the 1s ground state, index i will be omitted in the following.

The linear polarization fraction or the first Stokes parameter is defined for observation perpendicular to the beam axis by

$$P_{90}(\text{H}\alpha) = \frac{I_{\parallel} - I_{\perp}}{I_{\parallel} + I_{\perp}} \quad (7)$$

where I_{\parallel} and I_{\perp} are the light intensities with the electric field vector respectively parallel and perpendicular to the incident proton beam axis which was chosen as the quantization axis. As the collision plane contains the quantization axis, the collision is axially symmetric so that the density matrix is invariant under reflection in the scattering plane and thus cross sections for excitation of sublevels $+m$ and $-m$ are equal (Blum 1981). Neglecting the hyperfine-structure effects but including the depolarization by spin-orbit interactions (Percival and Seaton 1958), the H α line polarization is easily computed for capture or excitation from the $n = 3$ magnetic sublevel cross sections on using the definition (Syms *et al* 1975):

$$P_{90}(\text{H}\alpha) = \left[B_{31} \frac{\sigma_{3p_0} - \sigma_{3p_1}}{2} + 57 B_{32} \frac{\sigma_{3d_0} + \sigma_{3d_1} - \sigma_{3d_2}}{100} \right] \times \left[B_{30} \sigma_{3s_0} + B_{31} \frac{7\sigma_{3p_0} + 11\sigma_{3p_1}}{6} + B_{32} \frac{119\sigma_{3d_0} + 219\sigma_{3d_1} + 162\sigma_{3d_2}}{100} \right]^{-1}. \quad (8)$$

σ_{nl_m} is the partial cross section for either capture or direct excitation of sublevel nl_m and B_{3l} is the branching ratio of the H α emission probability to the total probability of emission from the $3l$ level, involving the Einstein coefficients:

$$B_{31} = \frac{A(3p \rightarrow 2s)}{A(3p \rightarrow 2s) + A(3p \rightarrow 1s)} = 0.1184 \quad (9)$$

$$B_{30} = B_{32} = 1. \quad (10)$$

3. Integral cross sections and polarization

The results for the total cross sections to the $n = 3$ level are compared in figure 1 with available experimental data (Detleffsen *et al* 1994, Hughes *et al* 1992). One observes an overall agreement, but as expected from previous work (Slim and Ermolaev 1994, Kuang and Lin 1996a, b) spurious oscillations appear in the excitation cross sections, particularly in the symmetric calculations. The same behaviour is found for excitation to $n = 2$. The TCAO-A calculations improve the results in the case of direct excitation whereas the TCAO-S calculations describe the capture process more accurately. Accordingly, all the following results are taken from TCAO-A or TCAO-S calculations for direct excitation or capture, respectively.

We wish to point out that the excited-state cross sections to the $n = 3$ levels are very small and the accuracy at the lower energies may still have some uncertainty. Better agreement has been found by Kuang and Lin (1996a, b) with the use of much larger basis sets. Nevertheless, we expect to obtain reasonably accurate results for the calculated differential cross sections and polarization.

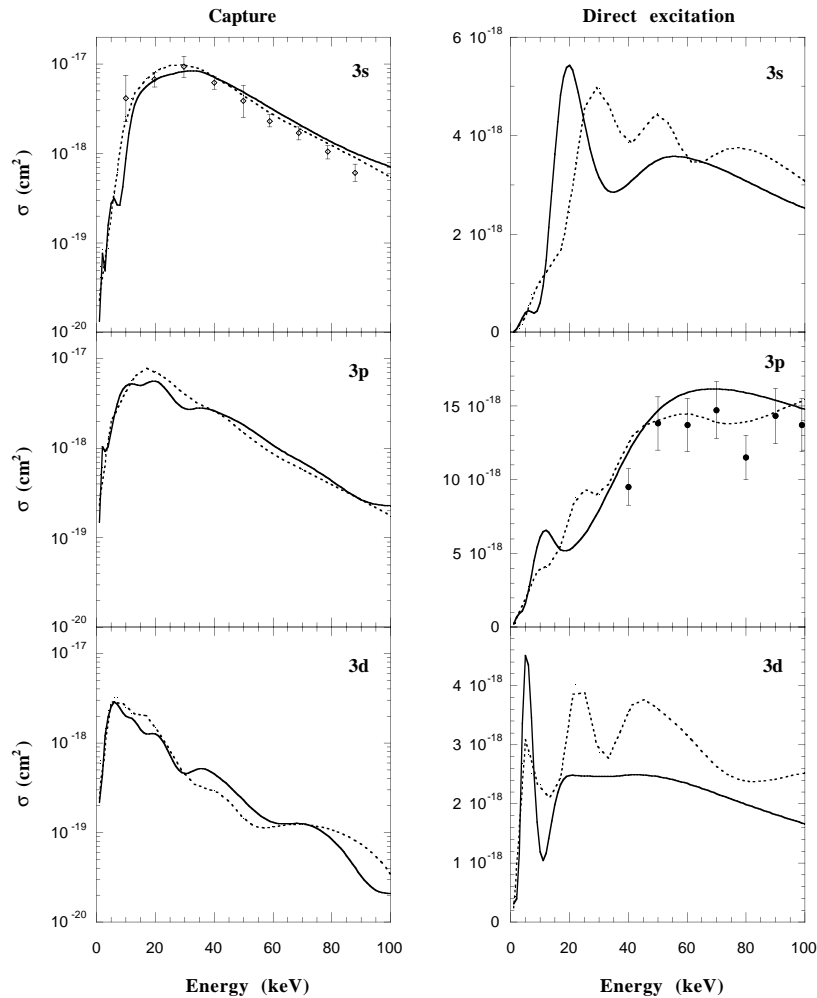


Figure 1. Capture and excitation cross section to $3l$. Theory: full curve, TCAO-A; dotted curve, TCAO-S. Experiment: \diamond , Hughes *et al* (1992); \bullet , Detleffsen *et al* (1994).

The present results for the polarization fraction after capture or direct excitation to the $n = 3$ level are shown in figure 2. The polarization fraction has the same order of magnitude for the two processes at the lower energies, but decreases much faster after 10 keV for the capture than for the excitation process. We obtain relatively good agreement with the experimental data from Werner and Schartner (1996) at higher energies ($E > 40$ keV). At these energies, capture gives no contribution so the experiment measures the polarized radiation emitted by directly excited atoms. We wish to point out that, due to the Doppler shift, the capture and excitation processes may contribute to different regions of the line profile. The polarization calculated here does not take into account other processes, such as excitation by radiation and depolarization by thermal collisions (Vogt *et al* 1997) which contribute to the total polarization observed in the centre of the $H\alpha$ line emitted during solar flares. However the thermal collision effects are very different whether we consider directly excited atoms or atoms excited by capture. For capture, the depolarization cross sections

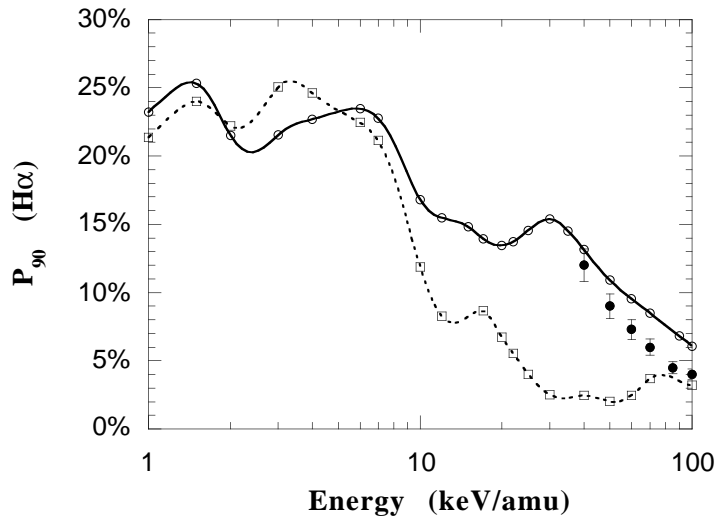


Figure 2. Polarization fraction of Balmer H α as a function of the collision energy. Theory: \circ , excitation; \square , capture. Experiment: \bullet , Werner and Scharfner (1996).

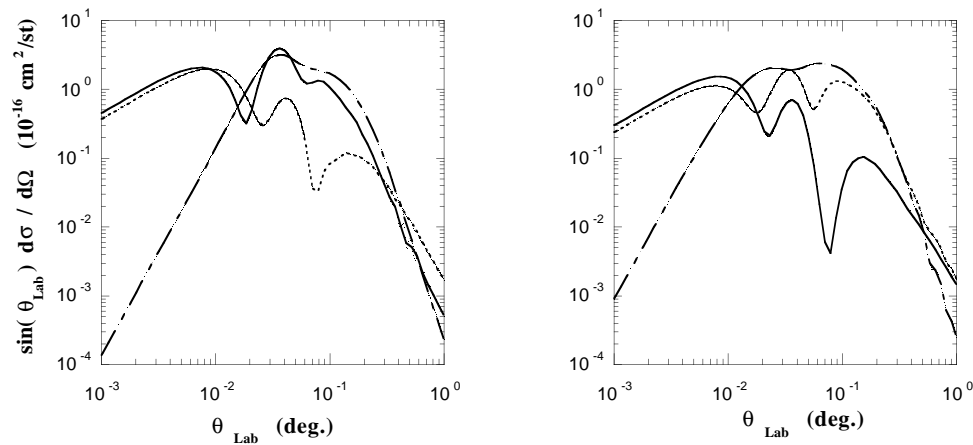


Figure 3. Reduced differential cross sections of the 3s and 3p magnetic sublevels in the case of capture (left) and direct excitation (right) as a function of the scattering angle for a 10 keV collision energy: full curve, 3s₀; dotted curve, 3p₀ and broken curve, 3p₁.

for collisions between the very fast excited atoms and the thermal electrons and protons of the medium are very small and excitation by radiation in the far wing is negligible. The calculated polarization is thus directly related to the observations.

4. Differential cross sections and polarization fraction

Figures 3 and 4 show the reduced differential cross sections $\sin(\theta_{\text{Lab}})d\sigma_{if}(\theta_{\text{Lab}}, E)/d\Omega$ of the different sublevels of $n = 3$ for a 10 keV collision energy. All of them have their maxima in the 10^{-2} – 10^{-1} degree range. The general behaviour of the differential cross sections for different energies is the same except that the direction of the largest cross section varies as

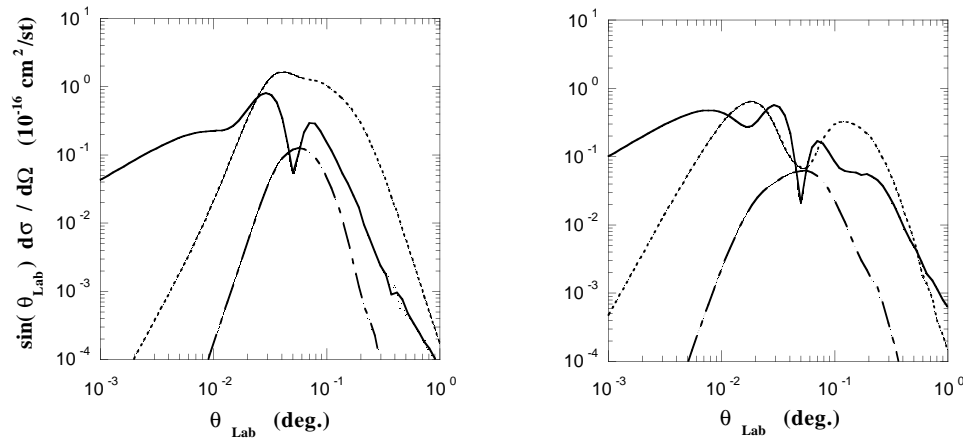


Figure 4. Reduced differential cross sections of the 3d magnetic sublevel in the case of capture (left) and direct excitation (right) as a function of the scattering angle for a 10 keV collision energy: full curve, 3d₀; dotted curve, 3d₁ and broken curve, 3d₂.

shown in figure 5. From these results it appears that the excited atoms have an anisotropic velocity distribution depending on the collision energy. Because of the Doppler effect, the emitted light intensity at a given wavelength λ in the wings of $H\alpha$ is directly related to the number of excited atoms in a given direction θ_{Lab} from the direction of the incident beam and thus to the differential cross section. The relatively large deflection angle for the smaller collision energies gives a possible diagnostic for the proton beam energy distribution by analysing the line profile.

The differential polarization fraction for Balmer alpha emission can be directly deduced from the present calculations. Our results for a collision energy of 1 keV are presented in figure 6. It appears that after some oscillations at smaller angles, the polarization fraction is almost constant around the maximum of the scattering angle. The same conclusions are reached for other energies, with the oscillation regime increasingly confined to smaller angles as the energy increases. The polarization fraction decreases slowly for larger angles which explains why the integrated polarization fraction is actually smaller than this maximum value.

5. Discussion and conclusion

In this paper, we have performed two types of TCAO close-coupling calculations. As expected (Kuang and Lin 1996a) the symmetric TCAO-S method leads to spurious oscillations in the excitation cross sections while the asymmetric TCAO-A calculation with all the pseudostates on the target centre gives more reliable excitation cross sections. The derived Balmer $H\alpha$ polarization fraction which displays a large oscillating structure in the TCAO-S calculation is clearly improved in the asymmetric approach. We wish to emphasize that the sign of the polarization fraction becomes negative for energies larger than 200 keV (Werner and Schartner 1996), and thus the observed polarization in solar flares may be due to proton beams of smaller energies.

The anisotropic velocity distribution of the protons gives rise to a Doppler shift of the emitted radiation which is directly related to the differential cross sections. This yields the angle at which the collision is the most efficient and therefore the velocity distribution of the

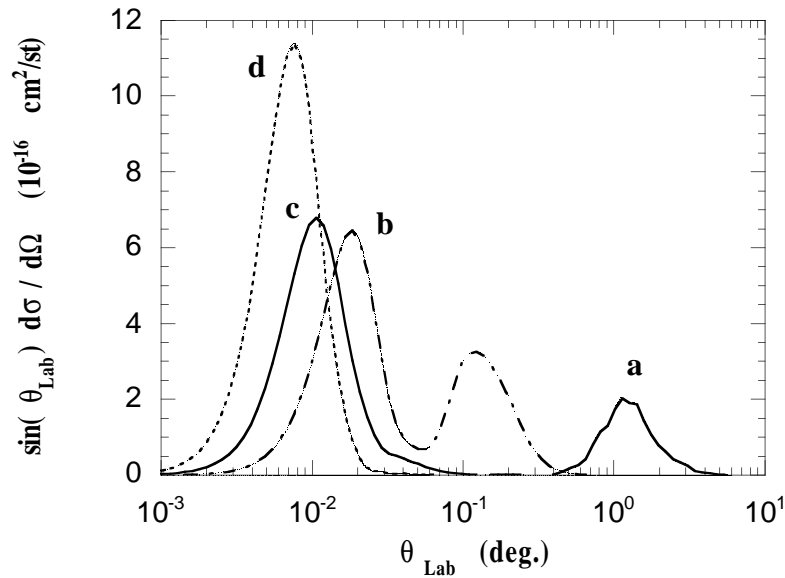


Figure 5. Reduced differential cross sections of the $3d_1$ magnetic sublevel in the case of direct excitation for four different values of the collision energy. **a**, $E = 1$ keV: $100 \times d\sigma/d\Omega$; **b**, $E = 10$ keV: $10 \times d\sigma/d\Omega$; **c**, $E = 25$ keV: $d\sigma/d\Omega$ and **d**, $E = 40$ keV: $d\sigma/d\Omega$.

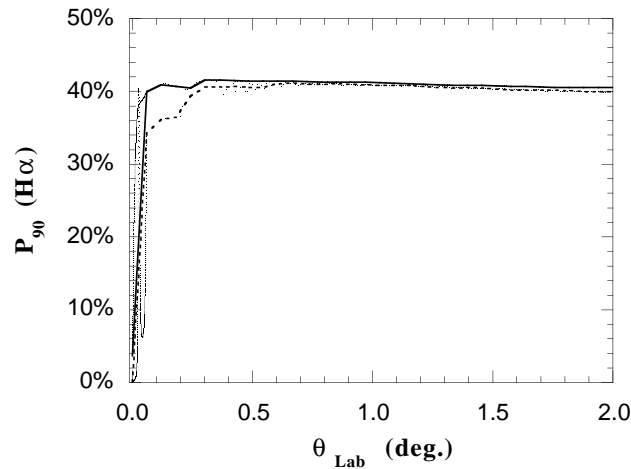


Figure 6. Differential polarization fraction for Balmer $H\alpha$ emission ($E = 1$ keV): dotted curve, excitation; full curve, capture.

excited atoms. As the collision energy varies from 1 to 40 keV, the maxima of the differential cross sections occur for angles varying from 1 degree to 10^{-2} degree. Due to these small deflection angles, the velocity of the atoms excited in a capture process is practically in the same direction as that of the incident proton beam. The corresponding emission of $H\alpha$ is shifted in the far wings of the line, according to the direction of observation. In the case of a direct excitation process, the recoil velocity of the excited atoms is almost perpendicular to the incident beam. Its order of magnitude is $v_p \theta_{\text{Lab}}$ where θ_{Lab} is the deflection angle and

v_p the velocity of the incident proton beam. For example, in the case of 1 keV incident protons, the recoil velocity is between 7 and 40 km s⁻¹; this leads to an important Doppler broadening of the Balmer $H\alpha$ line. Therefore the Doppler shift of the emitted radiation is a powerful diagnostic of the type of collision involved (all the data reported here are available upon request via e-mail). The differential polarization fraction is found to oscillate at very small angles and is almost constant for larger angles. These very small variations with the angle seem unlikely to be observed with accuracy.

Acknowledgments

CB and NF would like to thank Dr J-C Hénoux for helpful discussions regarding the observations. The computations were performed on the Convex and on the work stations of the Paris Observatory Computer Center. CDL is supported in part by the US Department of Energy, Office of Energy Research, Division of Chemical Sciences.

References

- Bates D R and McCarroll R 1958 *Proc. R. Soc. A* **245** 175
Blum K 1981 *Density Matrix Theory and Applications* (New York: Plenum)
Cheshire I M, Gallaher D F and Taylor A J 1970 *J. Phys. B: At. Mol. Phys.* **27** 4195
Detleffsen D, Anton M, Werner A and Schartner K-H 1994 *J. Phys. B: At. Mol. Opt. Phys.* **27** 4195
Dubois A, Nielsen S E and Hansen J P 1993 *J. Phys. B: At. Mol. Opt. Phys.* **26** 705
Fang C, Feautrier N and Hénoux J-C 1995 *Astron. Astrophys.* **297** 854
Fritsch W and Lin C D 1982 *J. Phys. B: At. Mol. Phys.* **15** 1255
———1983 *Phys. Rev. A* **27** 3361
Hénoux J-C, Chambe G, Smith D, Tamres P, Rovira M, Feautrier N and Sahal Bréchet S 1990 *Astrophys. J. Suppl.* **73** 303
Hughes M P, Geddes J, McCullough R W and Gilbody H B 1992 *Nucl. Instrum. Methods B* **79** 50
Kuang J and Lin C D 1996a *J. Phys. B: At. Mol. Opt. Phys.* **29** 1207
———1996b *J. Phys. B: At. Mol. Opt. Phys.* **29** 5443
Park J T, Aldag J E, George J M and Peacher J L 1976 *Phys. Rev. A* **14** 608
Percival I C and Seaton M J 1958 *Phil. Trans. R. Soc. A* **251** 113
Slim H A and Ermolaev A M 1994 *J. Phys. B: At. Mol. Opt. Phys.* **27** L203
Syms R F, McDowell M R C, Morgan L A and Myerscough V P 1975 *J. Phys. B: At. Mol. Phys.* **8** 2817
Vogt E, Sahal Bréchet S, Hénoux J C 1997 *Astron. Astrophys.* **324** 1211
Werner A, Schartner K-H 1996 *J. Phys. B: At. Mol. Opt. Phys.* **29** 125
Wilets L and Gallaher D F 1966 *Phys. Rev.* **147** 13